FULL PAPERS

Magnetic Resonance in Medicine 58:1099–1106 (2007)

Hyperpolarized C-13 Spectroscopic Imaging of the TRAMP Mouse at 3T—Initial Experience

Albert P. Chen,[1] Mark J. Albers,[1] Charles H. Cunningham,[2,3] Susan J. Kohler,[4] Yi-Fen Yen,[4] Ralph E. Hurd,[4] James Tropp,[4] Robert Bok,[1] John M. Pauly,[5] Sarah J. Nelson,[1] John Kurhanewicz,[1] and Daniel B. Vigneron[1*]

The transgenic adenocarcinoma of mouse prostate (TRAMP) mouse is a well-studied murine model of prostate cancer with histopathology and disease progression that mimic the human disease. To investigate differences in cellular bioenergetics between normal prostate epithelial cells and prostate tumor cells, in vivo MR spectroscopic (MRS) studies with non-proton nuclei, such as ^{13}C, in the TRAMP model would be extremely useful. The recent development of a method for retaining dynamic nuclear polarization (DNP) in solution permits high signal-to-noise ratio (SNR) ^{13}C MRI or MRSI data to be obtained following injection of a hyperpolarized ^{13}C agent. In this transgenic mouse study, this method was applied using a double spin-echo (DSE) pulse sequence with a small-tip-angle excitation RF pulse, hyperbolic-secant refocusing pulses, and a flyback echo-planar readout trajectory for fast (10–14 s) MRSI of ^{13}C pyruvate (pyr) and its metabolic products at 0.135 cm^3 nominal spatial resolution. Elevated ^{13}C lactate (lac) was observed in both primary and metastatic tumors, demonstrating the feasibility of studying cellular bioenergetics in vivo with DNP hyperpolarized ^{13}C MRSI. Magn Reson Med 58:1099–1106, 2007.

Key words: DNP; C-13; TRAMP; MRSI; flyback

The transgenic adenocarcinoma of mouse prostate (TRAMP) mouse is an established and well-studied murine model of prostate cancer (1,2). The histopathology of TRAMP mouse cancer tissue mimics that of human disease. TRAMP mice develop spontaneous progressive disease that begins with prostatic intraepithelial neoplasia (PIN) and then advances to frank carcinoma lesions in the prostatic lobes. The cancer also frequently metastasizes in this model to the lymph nodes (LN) and lungs, and, to a lesser extent, to the kidneys, adrenal glands, liver, and bone (2). The TRAMP model is being used in numerous laboratories to identify the molecular mechanisms associated with the initiation and progression of metastatic prostate cancer. Currently, almost all TRAMP studies use histopathology as the only parameter to evaluate the progression of the disease as well as the efficacy of the treatment agent being tested. Although this parameter is very useful and informative, the mouse has to be killed. Having a noninvasive, in vivo method would be valuable for following disease progression and treatment response in the same animal. TRAMP mice also serve as a good model system for testing new methods to characterize human prostate cancers.

Combined proton MRI and MR spectroscopic imaging (MRSI) exams have become routine clinical procedures for characterizing prostate cancer in humans (3–6). In particular, proton MRSI allows identification of changes associated with prostate cancer biomarkers, such as an increase in choline and a reduction in citrate. Single-voxel proton MRS data have been demonstrated in the TRAMP model (7), but this required a 7T animal MR system and an extremely long acquisition time (~2 hr for a single-voxel spectrum). Studying cellular bioenergetics in the TRAMP mouse would also benefit from in vivo MRS studies with non-proton nuclei, such as ^{13}C, but due to the low natural abundance of ^{13}C and its low sensitivity compared to the proton, the signal-to-noise ratio (SNR) is prohibitively low in small animals. With the recent development of a method for retaining dynamic nuclear polarization (DNP) in solution, high-SNR ^{13}C MRI and MRSI data have been demonstrated in rats following injection of a hyperpolarized ^{13}C agent (8–11). Substrates such as hyperpolarized ^{13}C pyruvate (pyr) and ^{13}C acetate allow unique access to observe fluxes in metabolic processes such as glycolysis and the citric acid cycle. In particular, hyperpolarized pyr labeled at the C_1 position has been injected into rats and pigs so that $^{13}C_1$ pyr and its metabolic products $^{13}C_1$ alanine (ala) and $^{13}C_1$ lactate (lac) can be observed (10,11) over a period of approximately 1 min after injection. This technique may enable the acquisition of ^{13}C MRS data with very high temporal resolution (on the order of seconds) and the observation of real-time, tissue-specific metabolic changes.

The MR properties of hyperpolarized agents are inherently different from those of endogenous nonhyperpolarized molecules. One of the most important considerations for imaging of hyperpolarized ^{13}C substrate is that the

[1]Department of Radiology, University of California–San Francisco, San Francisco, California, USA.

[2]Sunnybrook Health Sciences Centre, University of Toronto, Toronto, Canada.

[3]Department of Medical Biophysics, University of Toronto, Toronto, Canada.

[4]GE Healthcare Technologies, Menlo Park, California, USA.

[5]Department of Electrical Engineering, Stanford University, Stanford, California, USA.

Grant sponsor: National Institutes of Health; Grant number: R21 EB005363; NIH R01 EB007588. Grant sponsor: UC Discovery/GE Healthcare; Grant number: LSIT 10107.

*Correspondence to: Dr. Daniel B. Vigneron, Dept. of Radiology, Box 2512, University of California–San Francisco, 1700 4th St., Building QB3, Suite 102, San Francisco, CA 94158-2512. E-mail: daniel.vigneron@radiology.ucsf.edu

Received 20 October 2006; revised 12 February 2007; accepted 7 March 2007.

DOI 10.1002/mrm.21256

Published online 29 October 2007 in Wiley InterScience (www.interscience.wiley.com).

longitudinal magnetization consumed (by both T_1 relaxation and RF pulses) during an MR experiment is not restored by relaxation. Thus RF pulse sequences employed for MRI or MRS experiments of hyperpolarized ^{13}C must be able to utilize the prepolarized magnetization efficiently and quickly. One of the strategies for this situation is to use small-tip-angle excitation pulses to consume only a fraction of the magnetization for each *k*-space data point acquisition (11,12). In this study a double spin-echo (DSE) pulse sequence incorporating a small tip-angle excitation RF pulse and hyperbolic-secant refocusing pulses was used for MRSI of the ^{13}C substrate and its metabolic products. A flyback echo-planar readout trajectory was incorporated into this sequence in order to allow the rapid acquisition of multidimensional MRSI datasets (13).

The goal of this study was to use the developed DSE pulse sequence to determine the feasibility of acquiring high-spatial-resolution 3D ^{13}C MRSI data and 2D dynamic MRSI data in TRAMP and normal mice using hyperpolarized $^{13}C_1$-labeled pyr on a clinical 3T MR scanner.

MATERIALS AND METHODS

Polarizer and Materials

A prototype DNP polarizer that was developed and constructed by GE Healthcare (Malmö, Sweden) was used in this study. The polarizer was installed in the room adjacent to the MR scanner. The compound polarized was a mixture of pyruvic acid-1-^{13}C and the trityl radical (Tris[8-carboxyl-2,2,6,6-tetra[2-(1-hydroxyethyl)]-benzo(1, 2-d:4,5-d′)bis(1,3)dithiole-4-yl]methyl sodium salt) obtained from GE Healthcare (Oslo, Norway). The purity of the pyruvic acid was ~91% and the degree of labeling was >99%. TRIS/NaOH/EDTA dissolution medium was used to bring the final dissolved sample to the desired concentration and pH level. Two different concentrations of the hyperpolarized pyr solution (79 mM and 250 mM) were used in this study. An aliquot of the pyr solution was used to measure the percent polarization (ranging from 17% to 21% for these experiments), as well as the pH of the final solution (ranging from 6.5 to 8.0). In each of the mice studied, 0.35 ml of the final pyr solution was injected into the mouse over a 12-s period, followed by a 0.2-ml normal saline flush. The injection volume was approximately 10% of the mouse blood volume, which demonstrated no adverse effects. The protocol was approved by the UCSF Institutional Animal Care and Use Committee.

The polarization and subsequent dissolution were described previously (8). Briefly, the sample was loaded into a small cup constructed from PEEK, and then placed inside one end of a long Teflon tube. The sample was lowered into the variable-temperature insert (VTI) and then the VTI was evacuated to ~0.8 mbar to cool the sample to 1.2 K. The sample was then irradiated by microwave (~93.9 GHz) in a helium bath at a magnetic field of 3.35T for more than 1 hr. Just prior to the dissolution, the dissolution stick was filled with the dissolution medium, prepressurized with helium gas, and then heated. After the sample was polarized, and at the time of dissolution it was raised 10 cm from the center of the magnetic so that the sample was out of the helium bath. The dissolution stick was then inserted into the Teflon tube and connected to the sample cup to allow the hot solvent to be injected into the sample cup. A custom-made glass flask was used to collect the pyr solution. The glass flask was precooled in an ice bath so that the solution was approximately 40°C at the time of injection. The level of polarization was estimated using a custom-designed low-field NMR spectrometer that provided measurements of free induction decays (FIDs) from an aliquot of the dissolved solution.

RF Coil and Scanner

The RF coil used in the study was a custom-built dual-tuned ^{1}H-^{13}C coil with quadrature ^{13}C and quadrature ^{1}H channels that was designed and constructed for this study. It is based on an earlier design (14) in which a half-Helmholtz and a low-pass birdcage resonator (in this instance with eight rungs) were mounted on a single cylinder so as to share a pair of legs. The present coil differs from that reported in Ref. 14 merely in the addition of a second half-Helmholtz unit, to afford quadrature operation for protons. The diameter of the coil was 5 cm and the length of the coil was 8 cm to accommodate the significant size increase of the adult TRAMP mice as tumors developed. All studies were performed on a GE 3T scanner (Waukesha, WI, USA) equipped with multinuclear spectroscopy capability, including a broadband amplifier.

Pulse Sequence

A small-tip excitation followed by a DSE sequence was designed for fast spectroscopic imaging of ^{13}C hyperpolarized pyr and its metabolic products. An SE signal is desirable because it allows for phase-sensitive analysis of the spectroscopic data. Two hyperbolic secant pulses were used instead of the conventional RF refocusing pulses to achieve accurate refocusing and provide insensitivity to B_1 variations and/or minor errors in setting transmit gain (15). Since the hyperpolarized magnetization is not replenished by longitudinal relaxation, and any error in the refocusing pulse flip angle (FA) will contribute to the loss of magnetization, the adiabatic characteristic of these pulses is desirable for refocusing the spins in acquisitions that utilize hyperpolarized agents. Using a pair of adiabatic pulses is an important consideration since the pulse pair eliminates the frequency-dependent nonlinear phase that occurs when a single adiabatic pulse is used (16). The hyperbolic-secant refocusing pulse used had a bandwidth of 2.8 kHz, pulse duration of 10 ms, and maximum B_1 of 0.17 mT.

To allow acquisition of 3D or time-resolved 2D ^{13}C MRSI data within the very short time before the hyperpolarized magnetization decays by T_1 relaxation, a flyback echo-planar trajectory was implemented during signal readout to encode both spatial and frequency information (Fig. 1) (13,17). The flyback echo-planar trajectory was designed based on the 40 mT/m gradient amplitude and 150 mT/m/ms maximum slew rate available on the 3T MR scanner used in this study. The gradient waveform was designed for a 581-Hz spectral bandwidth to include ^{13}C lac, ^{13}C ala, and ^{13}C pyr without spectral aliasing. The designed bandwidth provided coverage of the ^{13}C metabolites while maintaining adequate SNR efficiency of the readout wave-

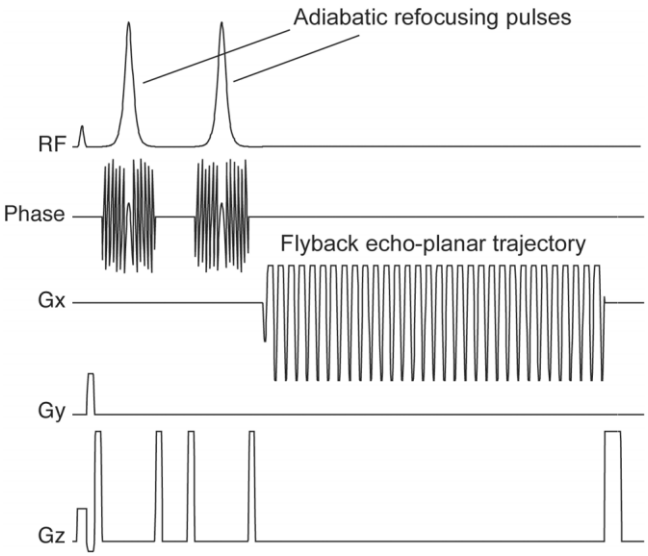

FIG. 1. The DSE pulse sequence designed for rapid ^{13}C MRSI data acquisition. Adiabatic refocusing pulses were incorporated to provide accurate 180° pulses and insensitivity to B_1 inhomogeneity, and to minimize the disturbance of the *z*-magnetization during refocusing. The flyback echo-planar trajectory was designed for 581-Hz spectral bandwidth and 5.4-mm minimum resolution in one dimension with standard phase-encoding in two other dimensions for 3D MRSI. With 2538 points sampled at 25000 Hz sampling rate, 16 *k*-space points were acquired during each readout, allowing a 16 × 8 × 8 MRSI acquisition in 10.24 s.

form. A total of 59 readout/rewind lobes were included during each readout for a spectral resolution of 9.83 Hz. With a readout filter of 25000 Hz/2538 points, 16 *k*-space points were acquired during each repetition time (TR), achieving a 16-fold decrease in acquisition time compared to conventional phase encoding with the same TR. The flyback readout trajectory was designed for a 5.4-mm minimum spatial resolution and an SNR efficiency of 61% (13).

Imaging Parameters

T_2-weighted anatomical images were obtained in all three planes using a fast SE (FSE) sequence. Axial and sagittal images were each acquired in 10 min with FOV = 10 cm, 192 × 192 matrix, slice thickness = 2 mm, and NEX = 6. Coronal images were acquired with FOV = 12 cm, 192 × 192 matrix, slice thickness = 1.5 mm, NEX = 8, and scan time = 10 min. The total imaging time required to obtain images in all three planes was thus approximately 30 min.

Time-resolved 2D ^{13}C MRSI data were acquired on one normal mouse from a 2D slice through the left mouse kidney using a 1 × 8 phase-encoding matrix with flyback echo-planar trajectory on the *x*-axis (16 × 8 effective matrix), 5.4 mm × 5.4 mm × 10 mm spatial resolution (0.292-cc voxel resolution), and a 43.2 mm × 43.2 mm FOV. The echo time (TE) was 35 ms, TR was 375 ms, and each 2D dataset was acquired in 3 s. The FA for the excitation pulses was 5°. A total of 20 time points were acquired.

3D ^{13}C MRSI data were acquired in 10–14 s in one normal mouse and four TRAMP mice using an 8 × 8 × 1 phase-encoding matrix with flyback echo-planar trajectory on the *z*-axis (8 × 8 × 16 effective matrix), 5 mm × 5 mm × 5.4 mm spatial resolution (0.135 cc voxel resolution), and 40 mm × 40 mm × 86.4 mm FOV to cover the mouse torso and abdomen. The TE for the 3D acquisition was 35 ms (readout began at the center of the second SE), the TR was 160 ms, and the total acquisition time was 10.24 s for three of the TRAMP mouse studies. For one TRAMP mouse, a TE of 140 ms was used with a 3D MRSI acquisition to obtain the second SE symmetrically (18) while using the same flyback echo-planar trajectory (readout was centered on the center of the second SE). In this case the TR was 215 ms and the total acquisition time was 13.76 s. A variable-FA (VFA) scheme was used for the small-tip-angle excitation pulse to effectively use all of the magnetization available (12).

Animals

All animal studies were carried out under a protocol approved by the UCSF Institutional Animal Care and Use Committee. TRAMP male mice were raised to 20–35 weeks of age. For each of the TRAMP mouse studied, intravenous access was established by a semipermanent jugular vein catheter placed during a surgical operation that typically occurred one or more days before the MR exam. Just prior to each study, the mouse was anesthetized with isoflurane (2–3%) delivered via O_2 flow at 1 liter/min. An i.v. extension tube was then attached to the main catheter and the animal was transferred to the scanner suite, placed on a 37°C heating pad, and positioned in the RF coil. Anesthesia was maintained by a continual delivery of isoflurane (1–1.5%) with oxygen (l liter/min) via a long tube to a nose cone placed over the mouse's snout. Respiratory rate and skin color were monitored by periodic visual inspection (facilitated by slots in the RF coil). One animal was also monitored during scanning by a specially designed, MR-compatible murine respiratory rate monitor (BioVet System, Summit Anesthesia Solutions). After the imaging studies, each animal was placed in an isolated cage and allowed to recover from the anesthesia.

One B6SJL male wild-type mouse was imaged at unknown age (~24 weeks) and 32.0 g body weight. One C57BL6/FVB male wild-type mouse was imaged at 20 weeks of age and 32.0 g body weight. Four C57BL6/FVB TRAMP mice supplied by the Roswell Park Cancer Institute (Buffalo, NY, USA) were imaged at 35 weeks, 23 weeks, 22 weeks, and 24 weeks of age, and 38 g, 34 g, 25 g, and 32 g of body weight, respectively (Table 1).

Data Analysis

All ^{13}C MRSI data were processed using custom MRSI processing software developed in our institution with modifications made specifically for this study. The raw data acquired with the DSE sequence were ordered as a 4D array, with the first dimension being *k*-space values in the flyback direction, the second being time decay, the third being one phase-encoding direction, and the fourth being

Table 1
Summary of the TRAMP and Normal Mice in This Study

Mouse	Age (weeks)	Weight (g)	Dose of pyruvate (ml/mM)	Polarization (%)	MRSI Study	Kidney lactate SNR	Primary tumor lactate SNR	Kidney lactate/ pyruvate ratio	Primary tumor lactate/pyruvate ratio
Normal 1	N/A	32	0.35/250	17.4	2D dynamic	26.9[a]	N/A	0.04[a]	N/A
Normal 2	20	32	0.30/79	20.9	3D	37.8	N/A	0.49	N/A
TRAMP 1	35	38	0.35/250	19.1	3D	83.6	44.9	0.08	0.12
TRAMP 2	23	34	0.35/79	17.3	3D	49.6	19.1	0.59	1.09
TRAMP 3	22	28	0.35/79	21.3	3D	63.7	62.7	0.99	1.57
TRAMP 4	24	32	0.25/79	19.6	3D–full echo	52.7	158.5	0.54	1.80

[a]The SNR and lactate/pyruvate ratio for the 2D dynamic study was derived from spectra acquired at the fifth time points, as shown in Fig. 2.
N/A = not applicable.

the other phase-encoding direction. The *k*-space points in the flyback dimension corresponding to the constant gradient portion of the trajectory were selected out and the data set was reordered so that time decay was the first dimension. The reordered dataset was then processed in the same manner used for the conventional 4D MRSI dataset, with the exception that the *k*-space points in the flyback dimension were each acquired at a slightly different time point (19). This was corrected during the 4D Fourier reconstruction using the fact that an origin shift in *k*-space is equivalent to a phase shift in the transformed domain. The time-domain signal was apodized by a 16-Hz Gaussian filter and zero-filled from 59 to 128 points. No apodization in the spatial domains was applied. The total reconstruction time on a SunBlade 1500 UNIX workstation (Sun Microsystems, Inc., Santa Clara, CA, USA) was approximately 5 s for 3D MRSI datasets acquired with the flyback echo-planar trajectory.

SNRs for all studies were calculated from a voxel in the kidney (also a voxel in the tumor in the TRAMP mice studies) using the peak height of the ^{13}C lac resonance and noise estimated from the right and left ends of the spectra that did not contain ^{13}C resonances.

RESULTS

Hyperpolarized ^{13}C MRSI spectra were obtained from two normal mice and four TRAMP mice using the new pulse sequence and coil developed for this study. The ^{13}C lac resonance in the mouse kidney was observed to have high SNR (26.9–83.6) in all studies, and to be high in the tumor for the TRAMP mice studies (Table 1). Alanine levels were often much lower than lac in most tissues (other than liver), and were often not observed in murine tumors. The lac/pyr ratio was also estimated in the kidney voxels and tumor voxels. In all four TRAMP mice studied, lac/pyr ratios were higher in the prostate cancers compared to the kidney.

The time-resolved 2D MRS images acquired from a normal mouse in a slice through the left mouse kidney demonstrated the time course of ^{13}C pyr uptake and conversion to ^{13}C lac in mouse kidney and muscle (Fig. 2). Substantial ^{13}C lac was observed in the kidney spectrum, with relatively lower ^{13}C lac observed in muscle. The representative 2D spectra array shown in Fig. 2b was collected from the fifth temporal time point. The SNR and lac/pyr ratios listed in Table 1 were also calculated from this spectral array.

^{13}C 3D MRSI were acquired at 0.135-cc nominal voxel resolution from a male wild-type mouse with spatial coverage throughout the body of the mouse in 10.24 s. Different ^{13}C metabolite profiles were observed in the mouse liver, kidney, and prostate (Fig. 3). Relatively high amounts of ala were observed in the liver compared to the kidney or normal mouse prostate. Relatively high levels of lac were observed in the kidneys. Lower levels of pyr and lac (^{13}C lac SNR mean = 17.2, ^{13}C pyr SNR = 20.9) and baseline level of ala were observed in the normal mouse prostate compared to the other tissue types. Respiratory motion did not appear to cause any adverse effects in either the T_2-weighted FSE images or the ^{13}C MRSI data in the anesthetized mice.

The 3D MRSI data acquired from a TRAMP mouse with a large primary tumor in the abdomen and an LN metastasis demonstrated a different metabolite pattern in the cancer regions as compared to the normal mouse prostate (Fig. 4). The ^{13}C MRSI spectra in kidneys were very similar in the normal mouse and the TRAMP mouse, with high levels of pyr and lac and relative low ala (Figs. 3c and 4b). However, in the TRAMP mouse the primary tumor and LN metastasis showed much higher relative lac levels compared to the kidney in the same animal and as compared to the normal mouse prostate (Figs. 3d and 4c and d).

When the DSE was used at a longer TE (140 ms) to acquire the symmetrically sampled SE in the 3D MRSI study (Fig. 5), the magnitude spectra had similar linewidth (22.6 Hz for lac) as compared to the pure absorption spectra (21 Hz for lac) acquired starting at the center of the echo (Fig. 4). Similarly to the short TE spectra, elevated lac (higher lac/pyr ratio) was observed in the TRAMP mouse prostate tumor compared to that observed in either the normal mouse prostate or the normal mouse kidney (Fig. 5).

DISCUSSION

This study demonstrates, for the first time, the feasibility of detecting the rapid cellular conversion of pyr to lac in a transgenic mouse model of prostate cancer using a hyperpolarized ^{13}C substrate. The methods developed in this study allowed the acquisition of 3D ^{13}C MRSI in approximately 10 s with a spatial resolution of 0.135 cm^3. Prom-

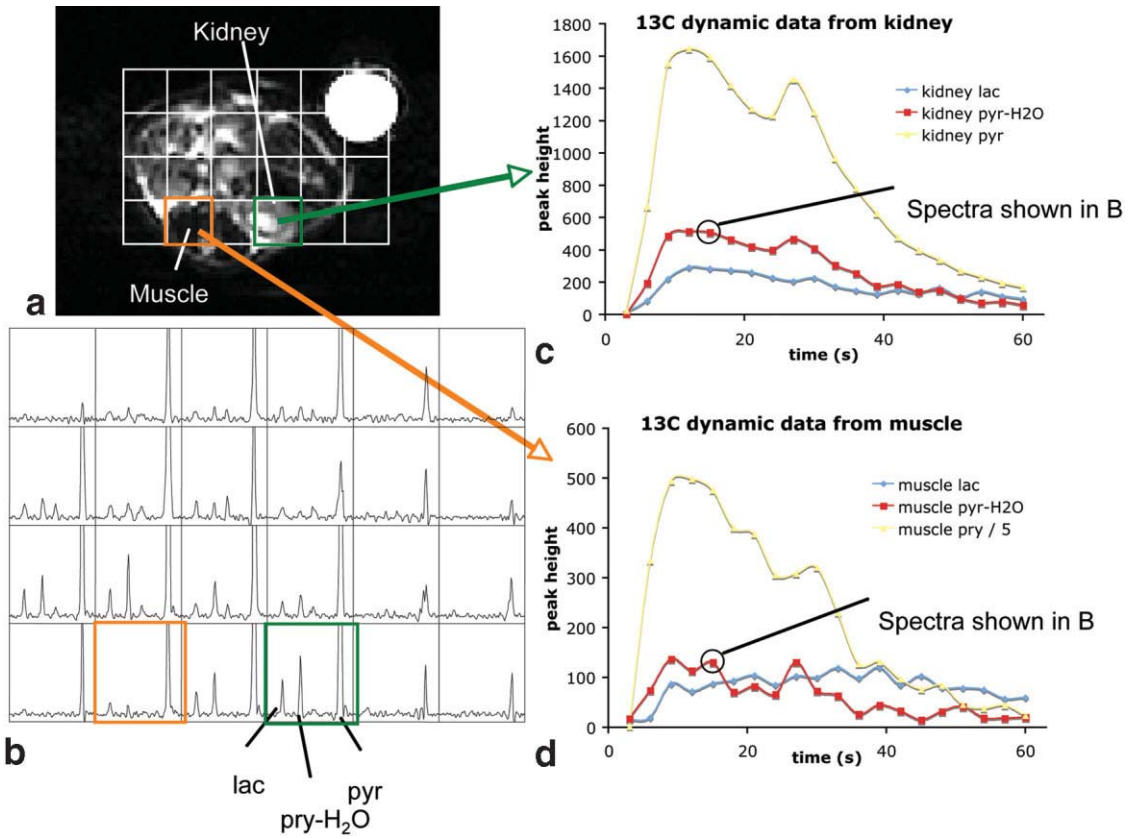

FIG. 2. ^{13}C time-resolved 2D MRSI data from a normal mouse (normal 1 in Table 1). The data were acquired from a 10-mm axial slice through the left mouse kidney, and the corresponding T_2-weighted FSE image is shown in **a** (upper left). Data acquisition began at the start of the injection, and 20 time points were acquired at 3-s temporal resolution. The spectra from the fifth time point are presented (**b**, lower left) to demonstrate the spatial distribution of the 2D MRSI data (0.292-cc voxel resolution). The dynamic curves from voxels centered on the kidney (**c**, upper right) and muscle (**d**, lower right) are also presented to show the time course of hyperpolarized ^{13}C pyr and lac.

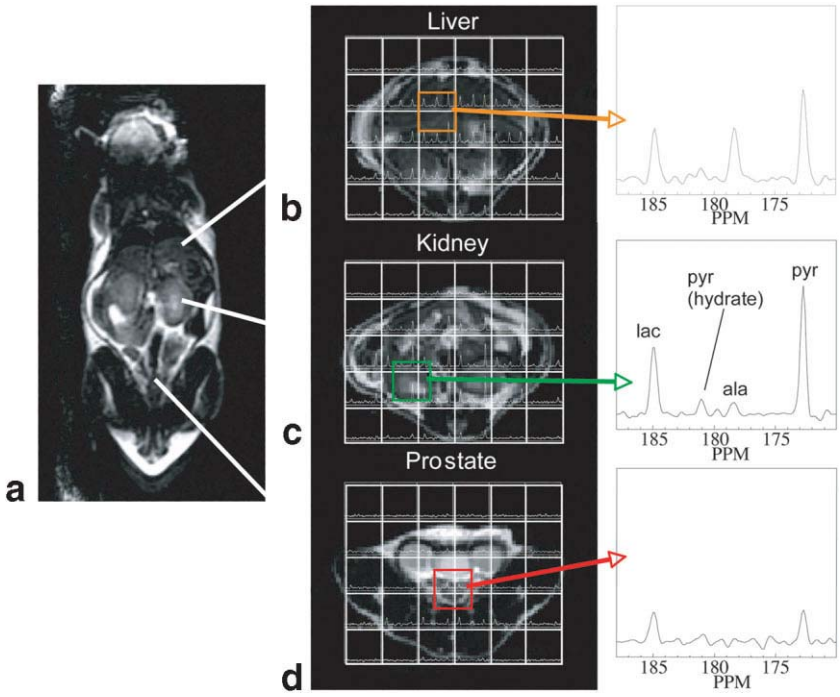

FIG. 3. **a:** A coronal T_2-weighted FSE image from a normal mouse (normal 2 in Table 1) demonstrating the relative location of the liver, kidney, and prostate is shown. **b–d:** Three axial images acquired through these organs are also shown with ^{13}C spectra obtained from the ^{13}C 3D-MRSI (0.135-cc voxels) overlaid on each image. Individual spectra from the liver (**b**), kidney (**c**), and prostate (**d**) are also presented on the right. High levels of pyr, ala, and lac were observed in liver, while the kidney demonstrated high lac and lower ala. Low levels of ^{13}C pyr as well as ^{13}C lac were seen in the normal mouse prostate.

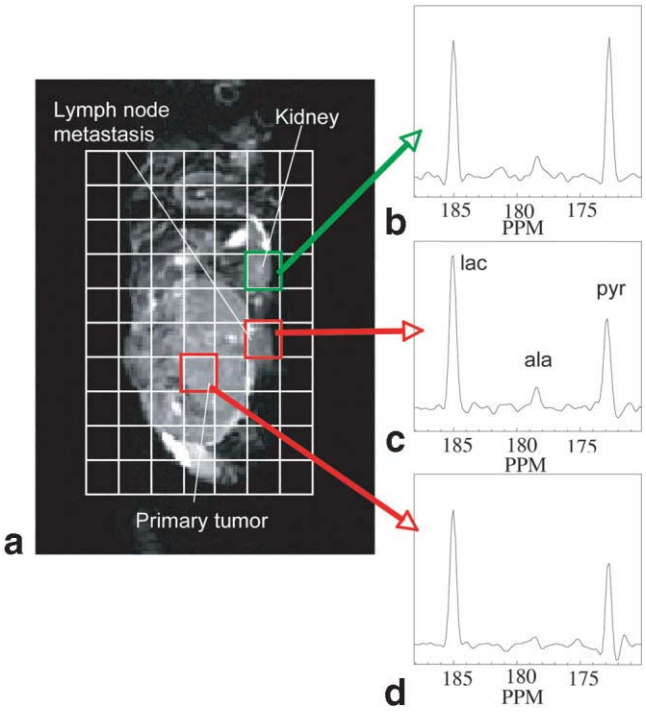

FIG. 4. **a:** T_2-weighted sagittal FSE image of a TRAMP mouse (TRAMP 3 in Table 1) studied. A large primary prostate tumor and an LN metastasis were observed and confirmed by subsequent postmortem dissection. 3D hyperpolarized ^{13}C MRSI data were acquired from the mouse 35 s after injection of 78 mM hyperpolarized ^{13}C pyr. While prominent ^{13}C pyr and ^{13}C lac resonances were observed in the kidney (**b**), elevated lac relative to pyr was observed in both the malignant LN (**c**) and the primary tumor (**d**).

inent ^{13}C lac resonances were detected in the liver, muscle, and kidney, but the highest lac levels were detected in TRAMP prostate tumors. This initial study indicates a strong potential for this relatively new in vivo metabolic imaging technique to become a powerful tool for monitoring the abnormal bioenergetics of prostate cancers.

Although MRSI of hyperpolarized ^{13}C agents requires a drastically different approach, it offers different and complementary information compared to proton MRSI. Prostate ^{1}H MRSI allows detection of small endogenous molecular markers (choline, spermine, and citrate) within the cytosol and extracellular spaces of the prostate at a steady-state level. The increase in choline and decrease in citrate level in prostate cancer tissue observed by ^{1}H MRSI is due to increased cell density, changes in cellular proliferation and phospholipid metabolism, and the loss of citrate production/secretion capacity that is unique to normal prostate epithelial cells (20).

In normal prostate tissue, citrate production (i.e., incompletion of the Krebs cycle) results in much lower energy production. The existence of substantial anaerobic metabolism and lower overall activity is unique to prostate epithelial cells (21). It can be speculated that the loss of citrate producing metabolism is associated with the increased need for energy in the process of malignancy. In addition, increased anaerobic metabolism can also play a role in supplying the energy requirements of cancerous tissue (22). If these and other metabolic transformations can be observed in vivo at different stages of malignancy, they may provide valuable information for the diagnosis, characterization, and treatment planning of prostate cancer.

By taking advantage of the DNP method to increase the MR sensitivity for ^{13}C substrates, this study demonstrates that changes in ^{13}C metabolite levels in the prostate tumor from the TRAMP model may be observed in vivo. Using the DSE MRSI sequence with flyback echo-planar encoding trajectory, time-resolved 2D and 3D spectra were obtained with very high SNR (Table 1). The high SNR obtained indicated that even higher spatial resolution may be feasible for future studies. Also, SNR may be further increased through improved RF coil design and higher-performance gradients. The use of a small tip angle with adiabatic refocusing to acquire hyperpolarized signal appeared to be robust, as demonstrated by very good spectral quality in all studies. Large FA with a refocusing pulse-train approach is another alternative for imaging of hyper-

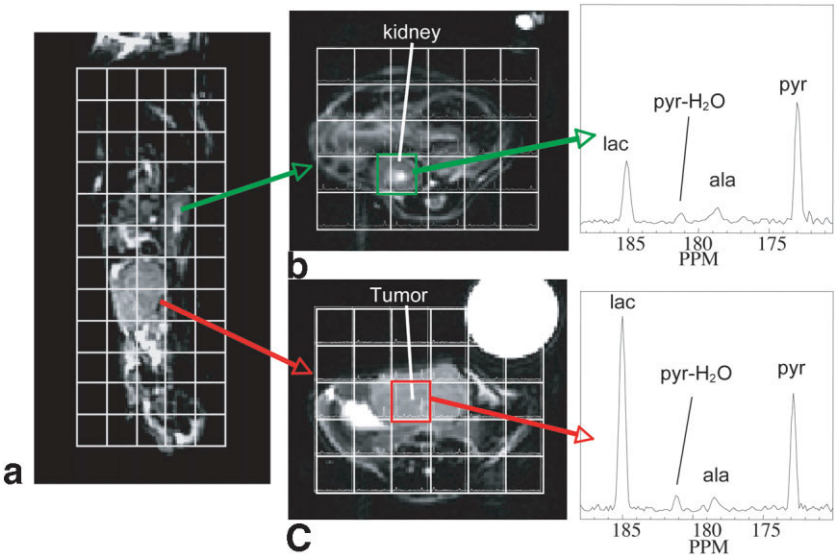

FIG. 5. T_2-weighted FSE images acquired from a 24-week-old TRAMP mouse (TRAMP 4 in Table 1) in sagittal (**a**) and axial planes are shown to localize the mouse kidney (**b**) and the large local spread of primary tumor (**c**). High-resolution ^{13}C 3D MRSI (0.135-cc voxel resolution) was performed after injection of 0.35 ml of 78 mM ^{13}C pyr. In contrast to the prior figures, a longer TE (140 ms) symmetric echo acquisition was used and magnitude spectra are shown. Different metabolic patterns were observed in the tumor as compared to the kidney. Elevated ^{13}C lac was observed in the region of mouse prostate cancer. Note that the magnitude spectra shown here have similar linewidths as compared to the pure-absorption, shorter-TE, half-echo spectra shown in Fig. 4.

polarized ^{13}C spins (23). In this approach, T_2 relaxation would dominate the signal decay during the experiment. It has been shown that a hyperpolarized ^{13}C substrate has much shorter apparent T_2 in vivo as compared to in solution (1.3 s vs. 18 s for bis -1,1-(hydroxymethyl)-1-^{13}C-cyclopropane-D_8) (23). Thus without accurate knowledge of the T_2 relaxation time of $^{13}C_1$-pyr in tissue, small-tip-angle excitation was chosen as a good approach for the 3D MRSI experiments in this study. The one TRAMP study performed with acquisition of the symmetric echo demonstrated the advantage of having the same linewidth in magnitude mode as compared to pure absorptive mode. It was not clear whether the longer-TE, full-echo acquisition showed improved SNR over the acquisition that acquired only the right-hand side of the echo when the kidney SNR was used for comparison (Table 1) (18,24). Measurement of in vivo T_2 relaxation times and a larger number of datasets acquired with both schemes are required to resolve whether the full-echo acquisition has a robust advantage in SNR for hyperpolarized ^{13}C MRSI.

The use of the flyback echo-planar readout enabled the acquisition of a high-resolution 3D MRSI dataset covering the entire mouse body in less than 14 s. This was highly significant for several different reasons. According to the dynamic studies shown previously (10,11) and the time-resolved 2D data shown in this study, it is crucial to choose an imaging window for the MRSI experiment before the decay of the ^{13}C signal via T_1 relaxation but after the ^{13}C pyr has been utilized by the tissue so its metabolite products and thus the tissue-dependent bioenergetics can be observed. This MRS imaging window is short by conventional MRI standards and is on the order of ~20 s, where the metabolite levels are stable and signal has not decayed significantly. In addition, to better depict the ^{13}C metabolic signatures of different tissues or organs, adequate spatial resolution (to reduce partial-volume effects) and a large encoding matrix (to cover the necessary anatomy) are required. The flyback readout trajectory designed for this experiment (5.4-mm minimum resolution) provides the capability for a MRSI matrix that is large enough to cover the mouse ($8 \times 8 \times 16$) within the desired imaging time.

Two different formulations of the ^{13}C pyruvic-acid/trityl radical mixtures were used in the study that resulted in two different concentrations (79 mM and 250 mM) of the hyperpolarized ^{13}C pyr solution. The injection volumes and injection rates were kept constant for all experiments. The pyr levels observed in the TRAMP study using the 250-mM formulation were much higher compared to the other three TRAMP studies using the 79-mM formulation (note the much lower lac/pyr ratio for the 250-mM study; Table 1), but the lac SNRs were similar. It can be speculated that since the ^{13}C pyr concentrations for both of the injected solutions were significantly higher than that of biological concentration (~0.2 mM), the lac SNR was limited partly by the ^{13}C pyr uptake rate and partly by its utilization within the tissue. Even at 79 mM, it is possible that the limit had been met. Understanding the possible trade-off in overall SNR and saturation of the biological metabolic rates may be an important consideration for future studies. In addition, the large differences in lac SNR in the tumor between different studies can presumably be attributed to differences in tumor stage in individual mice and the heterogeneity of the TRAMP model.

Although the lac/pyr ratio was observed to be fairly high (0.82), the normal prostate had much lower levels of both pyr and lac compared to the mouse liver, kidney, or tumor (Fig. 3). A complication of the interpretation of normal prostate lac/pyr ratios is the small size of the normal mouse prostate (~0.029 cm^3, measured in a prior study (7) from the same C57BL6/FVB male wild-type mouse used in this study) and the potential for partial voluming of surrounding tissues. In contrast, prostate tumors in TRAMP mice and other mouse organs were significantly larger than the spectroscopic voxels, and often multiple voxels could be placed within the tumor. In the TRAMP prostate tumor, the level of activity appeared to be elevated not only compared to normal mouse prostate, but to the kidney as well, with a much higher level of lac present. This observation may reflect the transformation from normal prostatic citrate-producing metabolism to malignant citrate-utilizing metabolism; however, the exact mechanisms that lead to the observed changes in the lac/pyr ratio still need to be elucidated. It is interesting to note that lac/pyr ratios were also higher in the tumor tissue compared to the kidney for all TRAMP studies (Table 1).

CONCLUSIONS

This study clearly demonstrates the feasibility of obtaining ^{13}C MRSI data with high SNR from normal and TRAMP mice after injecting the animals with hyperpolarized $^{13}C_1$ pyr. The small-tip-angle with adiabatic refocusing pulse sequence utilizing flyback echo-planar readout trajectory allowed rapid acquisition (in approximately 10 s) of large-matrix ^{13}C MRSI datasets. Different ^{13}C metabolic characteristics were observed in the mouse kidney, liver, normal prostate, and prostate tumor. This study shows that key bioenergetic metabolites in a prostate cancer model can be studied in the TRAMP mouse by MR using DNP to enhanced the signal from ^{13}C-labeled substrates.

REFERENCES

1. Greenberg NM, DeMayo F, Finegold MJ, Medina D, Tilley WD, Aspinall JO, Cunha GR, Donjacour AA, Matusik RJ, Rosen JM. Prostate cancer in a transgenic mouse. Proc Natl Acad Sci USA 1995;92:3439–3443.
2. Kaplan-Lefko PJ, Chen TM, Ittmann MM, Barrios RJ, Ayala GE, Huss WJ, Maddison LA, Foster BA, Greenberg NM. Pathobiology of autochthonous prostate cancer in a pre-clinical transgenic mouse model. Prostate 2003;55:219–237.
3. Kurhanewicz J, Swanson MG, Nelson SJ, Vigneron DB. Combined magnetic resonance imaging and spectroscopic imaging approach to molecular imaging of prostate cancer. J Magn Reson Imaging 2002;16:451–463.
4. Coakley FV, Qayyum A, Kurhanewicz J. Magnetic resonance imaging and spectroscopic imaging of prostate cancer. J Urol 2003;170(6 Pt 2):S69–75; discussion S75–66.
5. Mueller-Lisse UG, Swanson MG, Vigneron DB, Hricak H, Bessette A, Males RG, Wood PJ, Noworolski S, Nelson SJ, Barken I, Carroll PR, Kurhanewicz J. Time-dependent effects of hormone-deprivation therapy on prostate metabolism as detected by combined magnetic resonance imaging and 3D magnetic resonance spectroscopic imaging. Magn Reson Med 2001;46:49–57.

6. Scheenen TW, Gambarota G, Weiland E, Klomp DW, Futterer JJ, Barentsz JO, Heerschap A. Optimal timing for in vivo 1H-MR spectroscopic imaging of the human prostate at 3T. Magn Reson Med 2005;53:1268–1274.
7. Fricke ST, Rodriguez O, VanMeter J, Dettin LE, Casimiro M, Chien CD, Newell T, Johnson K, Ileva L, Ojeifo J, Johnson MD, Albanese C. In vivo magnetic resonance volumetric and spectroscopic analysis of mouse prostate cancer model. Prostate 2006;66:708–717.
8. Ardenkjaer-Larsen JH, Fridlund B, Gram A, Hansson G, Hansson L, Lerche MH, Servin R, Thaning M, Golman K. Increase in signal-to-noise ratio of > 10,000 times in liquid-state NMR. Proc Natl Acad Sci USA 2003;100:10158–10163.
9. Golman K, Ardenkjaer-Larsen JH, Peterson JS, Mansson S, Leunbach I. Molecular Imaging with endogenous substances. Proc Natl Acad Sci USA 2003;100:10435–10439.
10. Kohler SJ, Yen Y, Wolber J, Zandt R, Gram A, Ellner F, Thaning M, Chen AP, Albers M, Bok RA, Tropp J, Nelson SJ, Vigneron DB, Kurhanewicz J, Hurd R. Carbon-13 metabolic imaging at 3T using hyperpolarized 13C-1-pyruvate. In: Proceedings of the 14th Annual Meeting of ISMRM, Seattle, WA, USA, 2006 (Abstract 586).
11. Golman K, Zandt R, Thaning M. Real-time metabolic imaging. Proc Natl Acad Sci USA 2006;103:11270–11275.
12. Zhao L, Mulkern R, Tseng C, Williamson D, Patz S, Kraft R, Walsworth RL, Jolesz FA, Albert MS. Gradient-echo imaging considerations for hyperpolarized ^{129}Xe MR. J Magn Reson B 1996;113:179–183.
13. Cunningham C, Vigneron D, Chen A, Xu D, Nelson S, Hurd R, Kelley D, Pauly J. Design of flyback echo-planar readout gradients for magnetic resonance spectroscopic imaging. Magn Reson Med 2005;54:1286–1289.
14. Derby K, Tropp J, Hawryszko C. Design and evaluation of a novel dual-tuned resonator for spectroscopic imaging. J Magn Reson 1990;86:645–651.
15. Garwood M, DelaBarre L. The return of the frequency sweep: designing adiabatic pulses for contemporary NMR. J Magn Reson 2001;153:155–177.
16. Conolly S, Glover G, Nishimura D, Macovski A. A reduced power selective adiabatic spin-echo pulse sequence. Magn Reson Med 1991;18:28–38.
17. Posse S, Tedeschi G, Risinger R, Ogg R, Le BD. High speed 1H spectroscopic imaging in human brain by echo planar spatial-spectral encoding. Magn Reson Med 1995;33:34–40.
18. Dreher W, Leibfritz D. Fast proton spectroscopic imaging with high signal-to-noise ratio: spectroscopic RARE. Magn Reson Med 2002;47:523–528.
19. Nelson S. Analysis of volume MRI and MR Spectroscopic imaging data for the evaluation of patients with brain tumors. Magn Reson Med 2003;46:228–239.
20. Costello LC, Franklin RB. Novel role of zinc in the regulation of prostate citrate metabolism and its implications in prostate cancer. Prostate 1998;35:285–296.
21. Costello LC, Franklin RB. Bioenergetic theory of prostate malignancy. Prostate 1994;25:162–166.
22. Cornel EB, Smits GA, Oosterhof GO, Karthaus HF, Deburyne FM, Schalken JA, Heerschap A. Characterization of human prostate cancer, benign prostatic hyperplasia and normal prostate by in vitro 1H and 31P magnetic resonance spectroscopy. J Urol 1993;150:2019–2024.
23. Svensson J, Mansson S, Johansson E, Petersson JS, Olsson LE. Hyperpolarized ^{13}C MR angiography using True FISP. Magn Reson Med 2003;50:256–262.
24. Dreher W, Leibfritz D. A new method for fast proton spectroscopic imaging: spectroscopic GRASE. Magn Reson Med 2000;44:668–672.